*Solid State Phenomena*
*ISSN: 1662-9779, Vol. 343, pp 43-50*
*doi:10.4028/p-1i3w12*

*Submitted: 2022-09-04*
*Revised: 2022-12-02*
*Accepted: 2022-12-04*
*Online: 2023-05-30*

# 4H-SiC Full Wafer Mapping Image of CMP-Finished Sub-Surface Damage by Laser Light Scattering

Daichi Dojima[a*], Daichi Dansako[b], Mizuho Maki[c], Kohei Toda[d], and Tadaaki Kaneko[e]

Kwansei Gakuin University, 1, Gakuen Uegahara, Sanda, Hyogo, 669-1330, Japan

[a]d.dojima@kwansei.ac.jp, [b]dansako@kwansei.ac.jp, [c]gvv14386@kwansei.ac.jp, [d]k.toda@kwansei.ac.jp, [e]kaneko@kwansei.ac.jp

**Keywords:** Sub-surface damage, Laser light scattering, Wafer inspection, Mechanical process, Chemical mechanical polishing(CMP), Thermal etching, Epitaxial growth

**Abstract.** Developing an observation method for distributing sub-surface damage (SSD) on large-diameter 4H-SiC bulk wafers formed by mechanical processing can significantly improve the epitaxial and bulk growth processes. This study used a novel laser light scattering (LLS) technique to observe SSD distribution on a 6-inch 4H-SiC (0001) wafer. As a result, scattering intensity distributions similar to the grinding and lap-polishing traces and the shape of the jig used to hold the wafer during polishing were observed on the CMP-finished SiC wafer surface. Since the surface topography of the area was flat by a laser microscopy observation, it is assumed that this is the SSD. This result suggests that LLS can be a wafer inspection method that can observe SSD distribution. In addition, wafer inspection using LLS has demonstrated that it is possible to observe scratches, particles, and macrostep bunching. This method is anticipated to allow further optimization of the mechanical processing and thermal etching process prior to CVD epitaxial growth.

## Introduction

With the recent expansion of the standard 4H-SiC wafer diameter from 4 to 6 or even 8 inches, the development of high-speed, large-area evaluation technology is required. One such evaluation method is the cross-polarized imaging method, which uses polarized transmitted light to observe the strain distribution inside a wafer [1]. In addition, SICA, Candela, and PLI, which use ultraviolet light reflection, scattering, and photoluminescence phenomena to observe surface topography and crystal defect distribution, are also commonly used [2, 3]. In TEM observations of small areas, there is sub-surface damage (SSD) due to contact with diamond abrasive grains during wafer fabrication processes such as slicing, lap, and mechanical polishing. TEM measurements observe SSD as a scratch-like surface pattern and dense crystal defects at depths of approximately 100 nm [4]. This SSD has been reported to cause defect formation, such as triangular defects and surface roughening during CVD epitaxial growth [5]. It has been believed that this can be removed by performing a small amount of hydrogen etching prior to epitaxial growth in a CVD system. However, there are still difficulties in completely suppressing defect generation during epitaxial growth by controlling hydrogen etching [5, 6]. It is expected to become more challenging to maintain machining uniformity as the wafer diameter increases. This expectation may result in areas of greater SSD depth having a disparate distribution across the wafer. Therefore, developing a method to observe the distribution of SSD in large-diameter 4H-SiC bulk wafers will significantly improve the quality of epitaxial growth layers. To verify this hypothesis, we first developed the Laser Light Scattering (LLS) method, which enables the detection of SSDs on large-diameter wafers.

A schematic diagram of LLS inspection is shown in Fig. 1. The incident laser light has a wavelength of 355 nm, and a polarizer is used to select between S- and P-polarization. S- and P-polarized light indicates incident light with field oscillation orientations perpendicular and parallel to the plane of incidence, respectively. When using an oblique incidence laser beam near Brewster's angle, the P-polarized laser has more components that become transmitted light than the S-polarized

laser. Therefore, it is expected that information near the surface can be obtained if the incident light is S-polarized, and more internal information can be obtained if the incident light is P-polarized. To observe only scattered light, a photomultiplier tube, which is a detector, is placed at an angle where reflected light does not enter directly. The scanning technique involves rotating the wafer at high speed while moving the optical arrangement in the radial direction. This revolutionary method enables ultra-efficient observation of a 4-inch wafer in 2 minutes and a 6-inch wafer in 5 minutes. In this study, we used this LLS to verify whether it is possible to observe the distribution of the SSD by observing 6-inch SiC wafers with various surface processing states.

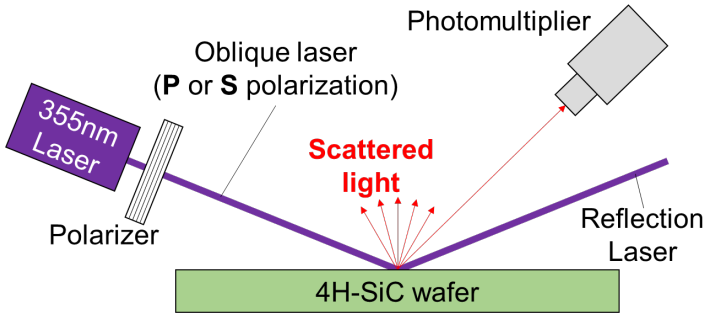


**Fig. 1.** Schematic of the LLS inspection system.

## Experiments

A 6-inch diameter 4H-SiC (0001) wafer, purchased from three major SiC vendors in 2021, was used as the sample for CMP finishing. In addition, SiC wafers, after each machining process, such as as-slice, lap, and MP, were used as samples with different SSD depths. As 6-inch SiC wafer samples with surface conditions after heat treatment, we prepared CVD epitaxial growth directly on wafers finished by CMP. As another sample after the thermal process, we prepared a SiC wafer etched with 8 μm thermal sublimation etching at 1800 °C by the Dynamic AGE-ing® method, which can control atomic-level surface flatness [7]. Observations were made using LLS to evaluate SSD on these SiC wafers.

The equipment for measuring LLS was fabricated by YGK corporation. In LLS observation of CMP wafers, the voltage applied to the photomultiplier tube is constant for all wafers. On the other hand, in LLS observation of the surface after machining and thermal processes other than CMP, the voltage applied to the photomultiplier tube is adjusted. Each of these samples was observed by cross-polarized imaging and parallel polarized observation using white transmitted light to measure internal wafer distortion and visual inspection, respectively. Transmission polarization imaging was performed with a Crystalline Tester CS1 from Ceramic Forum Co. In addition, laser microscopy and AFM observed the surface topography and step terrace structure, respectively. Laser microscopy measures surface topography by taking multiple images at different focal heights, with a minimum spatial resolution of 0.5 nm.

## Results and Discussions

First, the LLS observation was made from a 6-inch SiC wafer with Ra < 0.2 nm purchased from a major vendor in 2021. Fig. 2 shows the LLS mapping images, the polarized light microscope images, and the parallel polarized observation images of a 6-inch SiC wafer with a CMP-finished surface. Figs. 2 (a) and (b) are the results of the LLS observation with S- and P-polarized light, respectively. In the case of the S-polarized light, a scattering intensity distribution spreading in a ripple pattern was observed from the upper right corner of the wafer. On the other hand, in the case of P-polarized light, a concentric scattering intensity distribution centered in the middle of the wafer was strongly observed. Here, this concentric scattering intensity distribution is obtained by observing a deeper region than the rippled scattering intensity distribution observed with S-polarized light because the incident light of P-polarized light is more transmitted than that of S-polarized light. The strain distribution inside the wafer in Fig. 2 (c), in which the same substrate was observed by cross-polarized light imaging, showed bright contrasting distortion areas in the upper right and lower right and asterisk-shaped distortion throughout the wafer. Since cross-polarization imaging uses transmitted light, these

distortions are thought to have been introduced during SiC ingot growth. Furthermore, Fig. 2 (d), in which the parallel polarized observation image was obtained for the same substrate using white transmitted light, shows a carbon facet region with a high nitrogen concentration that exhibits a dark contrast at the center.

The scattering intensity distribution observed in the LLS mapping image is shown to be quite different from the strain distribution observed in transmitted light. This suggests that LLS observes light scattered at the surface and that a strain state exists below the surface that is quite different from that inside the wafer. The scattering intensity distribution observed by the LLS S-polarized light is close to linear traces in the lap or the grinding process [8, 9]. The scattering intensity distribution observed in P-polarized light is close to the shape of the jig that supports the wafer by the vacuum chuck during MP and CMP. Those results suggest that the scattering intensity distribution observed in the LLS mapping image is SSD introduced to the SiC wafer sub-surface by the machining process. So, it is expected that the SSD from the Lap and Grinding processes and the thermal distortion from the high processing pressure applied to the SiC wafer in the MP and CMP processes will remain on the sub-surface of the commercially available wafer after CMP. The results also suggest that internal wafer distortion and differences in nitrogen concentration do not affect surface processing.

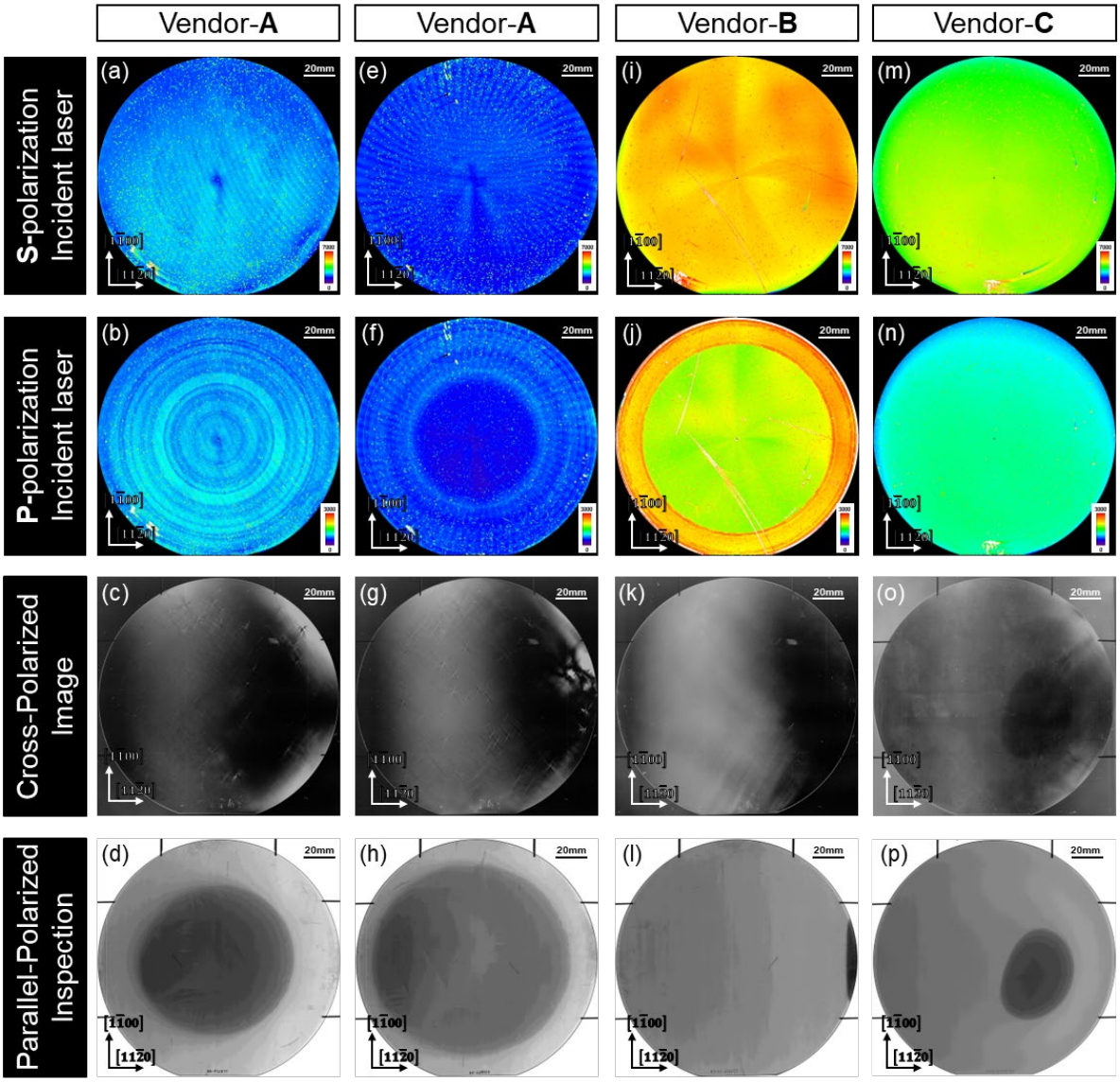


**Fig. 2.** Observation results of CMP-finished 6-inch 4H-SiC wafers purchased in 2021 from vendors **(a)-(h)** A for two wafers and **(i)-(l)** B and **(m)-(p)** C for one wafer. For each wafer, LLS with S- and P-polarized light, cross-polarized imaging, and parallel polarized observation were performed. the color scale of the LLS mapping image indicates the intensity of scattered light.

Figs. 2 (e)-(h) show observation results on different wafers purchased from Vendor A. The LLS observation with S-polarized light showed a scattering intensity distribution that spread from the center of the wafer in a vortex-like pattern. In addition, a scattering intensity distribution that spread from the top of the wafer in a rippled pattern was observed. In the case of p-polarized light, a circular area with φ60 mm in which almost nothing was observed. In contrast, the SSD distribution similar to the S-polarized light image was observed outside of this area. In the cross-polarization and the parallel polarized observation images of the wafer, stark contrast was observed in the upper right and lower right, and a dark contrast C-facet was observed in the center, respectively. However, compared with the LLS mapping image, no relationship was found in their scattering intensity distribution as in the first wafer. Comparing the LLS mapping images of the two Vender-A wafers, there is a significant distributional difference in both S- and P-polarization measurements. In other words, SSD distribution is expected to vary widely from wafer to wafer, even for wafers from the same vendor.

Figs. 2 (i)-(l) show the results of the wafer measurements for Vendor B. In the LLS mapping image of the wafer measured with S-polarized light, four spiral-shaped scattering intensity distributions extending from the wafer center were observed. In addition, significant scattering intensity, linear patterns as long as 100 mm, and small dot patterns were identified. These line- and dot-shaped patterns were observed in the same positions in p-polarized light. In contrast, the ripple scattering intensity distribution seen in S-polarized light observation could not be confirmed in P-polarized light. A circular scattering intensity distribution with a scattering intensity of about 120 mm radius was identified in the center of the wafer. It was also found that the wafer from Vendor B had a higher scatter intensity than that from Vendor A. These suggested that SSD depth and distribution varied widely from vendor to vendor. In the cross-polarized image, there was no high contrast or asterisk-shaped distortion, as seen in Vendor A.

Figs. 2 (m)-(p) show the observation results of a wafer from Vendor C. As seen from the P- and S-polarization in the LLS mapping image, there was no scattering intensity distribution as in Vendor A and Vendor B. Furthermore, no other characteristic scattering intensity distribution was observed. It should be noted here that the average scattering intensity is equal to or higher than that of the Vendor A wafer. Those results confirm that the SSD depth and distribution vary significantly from vendor to vendor, even for the same CMP-finished wafer. Furthermore, in the cross-polarization and the parallel polarized observation images, the internal strains and nitrogen concentration distribution of wafers from Vendor C significantly differ from Vendor A and Vendor B. In summary, these results indicate that the scattering intensity distribution observed in LLS, which appears to be introduced by mechanical processing, varies from vendor to vendor and even within a vendor from wafer to wafer and is independent of the strain and nitrogen concentration distribution inside the wafer.

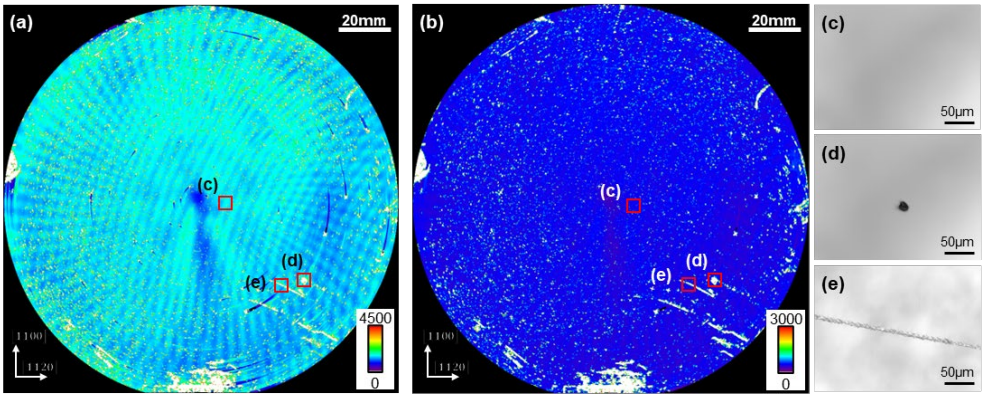


**Fig. 3.** LLS mapping images of CMP-finished SiC wafers purchased from Vendor A in 2021, observed with **(a)** S- and **(b)** P-polarized light, respectively. Laser microscope images of areas showing **(c)** rippled, **(d)** dotted, and **(e)** linear patterns in the LLS mapping images.

Figs. 3 (a) and (b) are the LLS mapping images of the Vendor A wafer with S- and P-polarization, respectively. Figs. 3 (c)-(e) are the laser microscope images of areas with characteristic patterns in the LLS mapping image. Fig. 3 (c) shows the areas where the rippled scattering intensity distribution is visible only in the S-polarized light observation. This area shows very high flatness in laser

microscopy observation. These results indicate that the rippled distribution observed at the S-polarization observation image of LLS is due to scattering phenomena unrelated to surface topography. Fig. 3 (d) is the laser microscopy image of the areas where dotted scattering intensity distribution was observed in both S- and P-polarization observations. The laser microscope images of this area showed particles about 20 μm in diameter. Fig. 3 (e) shows the laser microscope image of the area where linear scattering intensity distribution was observed in both the S- and P-polarized light observation images. This laser microscope image could observe a scratch of slightly less than 10 μm. These results suggest that the scattering intensity distribution showing significant scattering intensity, visible in both S- and P-polarization, is related to scattering phenomena caused by surface morphology.

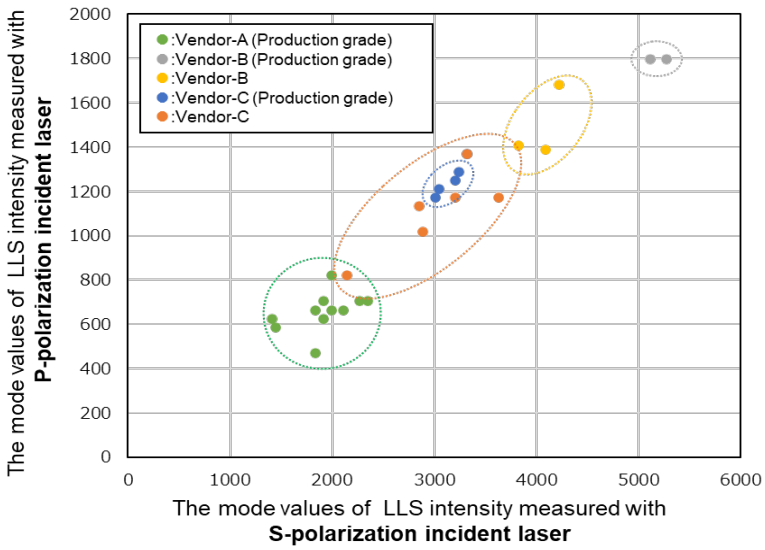


**Fig. 4.** Graph of the mode values of LLS intensity measured with S- and P-polarization incident laser for 26 CMP finished 6-inch 4H-SiC (0001) wafers of Vendor A-C.

Histograms of scattering intensities were created from LLS mapping images of 26 CMP-finished SiC wafers purchased from Vendor A-C using S- and P-polarized light. The mode values of the histograms are plotted in Fig. 4. The graph shows a positive correlation between the scattering intensity in S-polarized light and that in P-polarized light observation. The graph also showed that the scattering intensity values were grouped by vendor and wafer grade, as enclosed by the dotted line. From the previous results, it can be assumed that the greater the scattering intensity, the greater the magnitude of the SSD. Therefore, it can be inferred that the SSD remains after CMP is deeper in the order of Vendors A, C, and B. This result indicates that the reproducibility of the LLS intensity is sufficiently high to allow such a classification. It is also suggested that the size of SSDs introduced into each wafer can be non-destructively inspected by creating a histogram of the LLS mapping image.

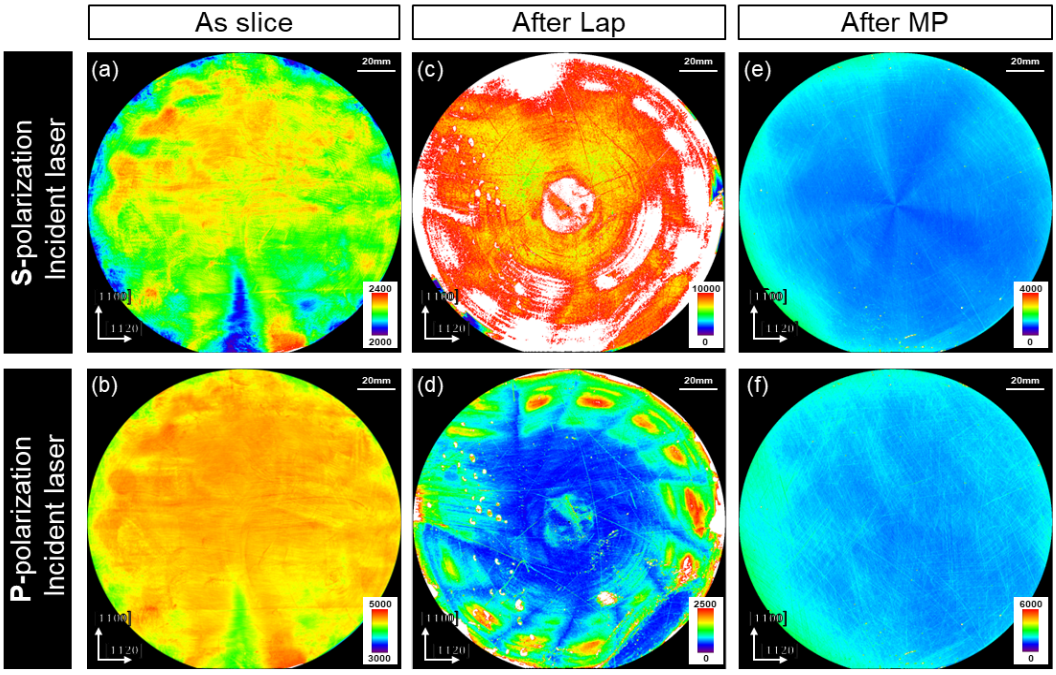


**Fig. 5.** LLS mapping images of the 4H-SiC(0001) wafer after each **(a)-(b)** as-sliced, **(c)-(d)** Lap, and **(e)-(f)** MP process measured with S- and P-polarization, respectively.

Next, the application of the LLS to SiC wafers at different mechanical processing stages was verified. Fig. 5 shows the LLS mapping images of SiC wafers after as slice, lap, MP, and CMP, respectively. Figs. 5 (a) and (b) are the LLS mapping images of as-slice substrates observed with S- and P-polarization, respectively. A line-shaped scattering intensity distribution was observed. The shape suggests that the scattering is due to surface roughness caused by the wire-saw slicing process [10]. No scattering intensity distribution other than slice marks was observed. Figs. 5 (c) and (d) show the results of measuring the wafer after the lapping process. Linear and spiral scattering intensity distribution were observed in both the S- and P-polarization LLS mapping images. This spiral scattering intensity distribution closely resembles the surface geometry observed in the lapping and grinding process [9]. Figs. 5 (e) and (f) show the results of the LLS mapping images of the wafer after the MP process. Short linear scattering intensity distribution introduced throughout the wafer was observed in both S- and P-polarized light observation.

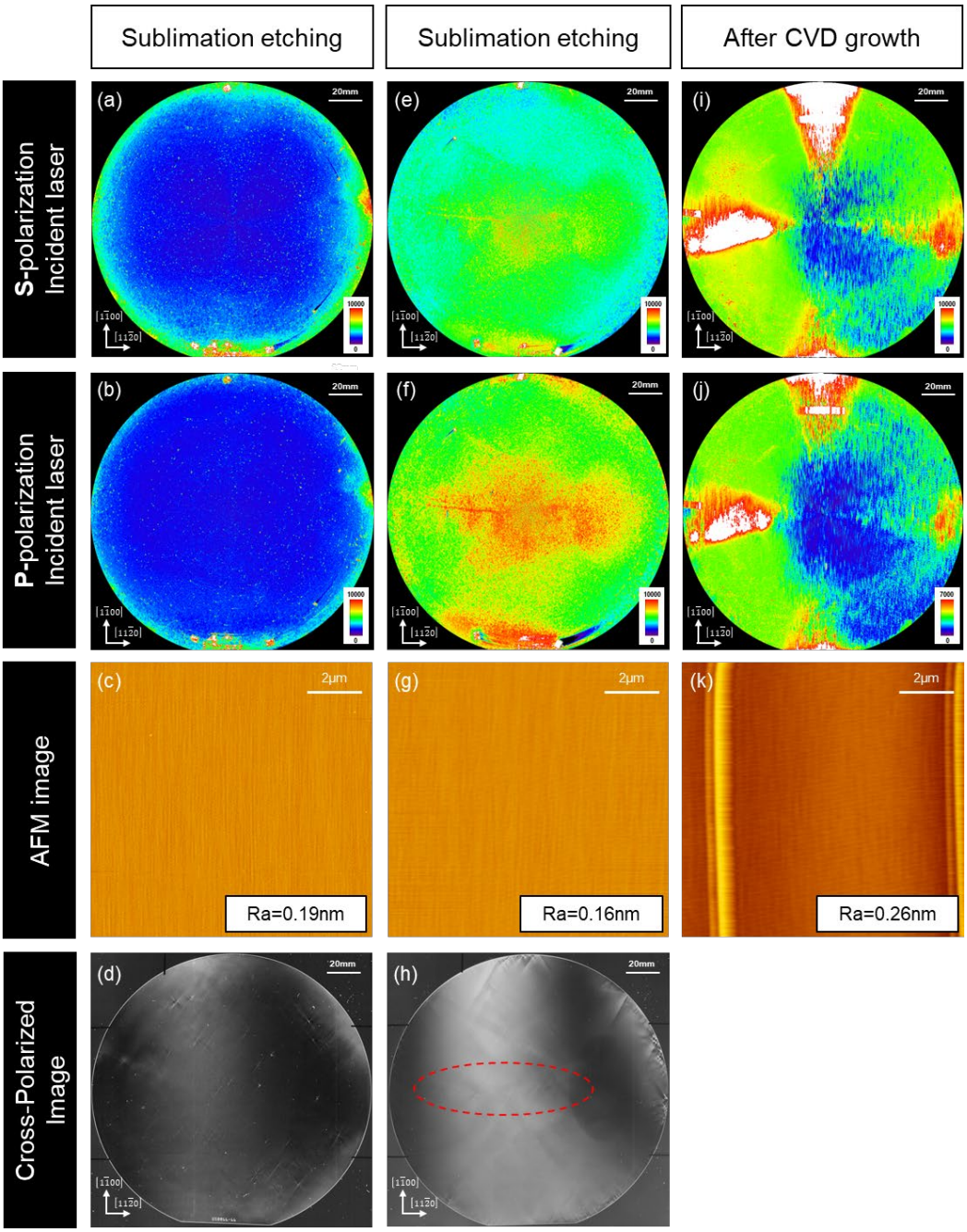


**Fig. 6. (a)-(d)** and **(e)-(h)** LLS mapping, AFM, and cross-polarization images of SiC wafers after sublimation etching. **(a)-(d)** and **(e)-(h)** are SiC wafers used for the observation in Fig. 3 and wafers made by another vendor, respectively. **(i)-(k)** LLS mapping and AFM images of CVD-grown surfaces directly on CMP wafers. All AFM images were measured at the center of each wafer.

As mentioned above, the linear scattering intensity distribution observable in both the S- and P-polarization at the LLS mapping image is a scratch. It is estimated that these scratches were introduced by contact with diamond abrasive grains during the MP process. For as-sliced and post-Lap, MP wafers, the LLS mapping images for both S- and P-polarized light are similar, and it can be inferred that in wafers with rough surfaces, the scattering due to surface roughness accounts for most of the information. Thus, it was found that for wafers with rough surfaces, it is possible to observe mainly surface roughness, and when the surface flatness reaches about CMP (Ra<0.2nm), information about SSD can be obtained at the same time.

We next verified the LLS observation results after thermal sublimation etching. LLS mapping images of CMP wafers with thermal sublimation etching are shown in Fig. 6 (a)-(c). Here, Figures 6(a)-(c) show the LLS and AFM observation results after the thermal sublimation etching of the wafer used for the observation in Figure 3. The wavy and spiral-like scattering intensity distributions seen in the S-polarized light observation before etching have been completely eliminated. Scratches and particle-like patterns that were visible in both S- and P-polarized light are also no longer visible. As can be seen in Fig. 6 (c), the surface roughness Ra after etching is 0.19 nm, which is as flat as the wafer level after CMP. Here, the AFM image is measured at the center point of the wafer. Fig. 6 (d) shows the cross-polarized image of this wafer. Low-density asterisk-shaped distortions were observed over the entire wafer. These results suggest that SSD, scratch, and particle removal effects are measurable by LLS in thermal sublimation etching with sufficient flatness.

Figs. 6 (e)-(h) show the LLS, AFM, and cross-polarized images of the surface of a thermally sublimated etch on a CMP-finished SiC wafer obtained from another vendor. High scattering intensity areas were observed near the center of the wafer for both S- and P-polarized light observation. AFM measurements showed that the surface roughness Ra was 0.16 nm, a controlled wafer-level flatness after CMP. From the cross-polarized image, careful observation reveals a cluster of dense asterisk-shaped distortions in the area circled by the red dotted line. This region is the same area where the LLS scattering intensity is high. These results suggest that LLS observation can visualize internal wafer distortion by removing SSD in a thermal sublimation etching that maintains sufficient planarity.

Finally, we examined what is obtained when LLS observations are made after CVD epitaxial growth, which is the most common thermal process of the SiC wafer. Figs. 6 (i) and (j) are the LLS mapping images after CVD epitaxial growth. The S- and P-polarized light observations showed scattering intensity distribution with a width of 10 mm, and a length of 20 mm was observed on the top of the wafer. This scattering intensity distribution can be inferred from its shape to be a macrostep bunching shape generated from scratches [5]. In addition, a linear scattering intensity distribution along the <1-100> direction with a length of about 10 mm was observed at the entire wafer. This scattering intensity distribution is due to the macro step bunching, which is also seen in the AFM image. Here, the triangular distribution observed in the LLS mapping image, which extends from the wafer center in the <1-100> and <11-20> directions, is not essential because it is a noise introduced during the LLS observation. Thus, the LLS observation was shown to be useful as a surface topography inspection method after CVD epitaxial growth.

## Summary

In this study, a new LLS-based observation technique was used to evaluate the processing damage on the sub-surface of a 6-inch 4H-SiC wafer purchased in 2021. In this observation method, the depth of the measurement area is varied by changing the incident laser light to S- or P-polarized light, and the SSD distribution of different strain distributions for each wafer or vendor is successfully observed. In the presence of surface roughness, such as scratches, particles, and macrostep bunching, the same scattering intensity distribution was obtained for both S- and P-polarized images. Then, in the CMP and thermal etching surfaces with sufficiently flat surfaces, the distribution of SSDs and their removal, which had not been observed before, were observed. Furthermore, LLS observation is promising as a total inspection method because it requires only about 5 minutes to inspect the entire surface of a 6-inch wafer by rotating the wafer and scanning it. Adopting this method makes it possible to optimize the mechanical and thermal etching processes prior to CVD epitaxial growth, resulting in a higher-

quality epitaxial growth layer. This method is applicable not only to SiC wafers but also to many other semiconductor materials. Our future work includes mapping the SSD observed in the LLS to general strain evaluation methods such as Raman, exploring measurable depths, and investigating the quantitativeness of the strain.

**Acknowledgments**

The authors are grateful to Toyota Tsusho Corporation for funding and technical support and YGK Corporation for equipment support.

**References**

[1] X. Ma, M. Parker, and T.S. Sudarshan, Nondestructive defect delineation in SiC wafers based on an optical stress technique, Appl. Phys. Lett. 80 (2002) 3298-3300.

[2] G. Chung, I. Manning, A. Soukhojak, M. Gave and C Lee, Decoration and Density Increase of Dislocations in PVT-Grown SiC Boules with Post-Growth Thermal Processing, Materials Science Forum. 1062 (2022) 246-250.

[3] M. Odawara, K. Kamei, Y. Miyasaka, T. Yamashita, S. Takahashi, Y. Kageshima, K. Momose, H. Osawab, and T. Sato, Defects grouping and characterizations of PL-imaging methods for 4H-SiC epitaxial layers, Materials Science Forum. 778-780 (2014) 382-385.

[4] H. Sako, H. Matsuhata, M. Sasaki, M. Nagaya, T. Kido, K. Kawata, T. Kato, J. Senzaki, M. Kitabatake, and H. Okumura, Micro-structural analysis of local damage introduced in subsurface regions of 4H-SiC wafers during chemo-mechanical polishing, J. Appl. Phys. 119 (2016) 135702.

[5] M. Sasaki, H. Matsuhata1, K Tamura, H Sako, K Kojima, H Yamaguchi, and M Kitabatake, Synchrotron X-ray topography analysis of local damage occurring during polishing of 4H-SiC wafers, J. Appl. Phys. 54 (2015) 091301.

[6] R. Anzalone, N. Piluso, M. Salanitri, S. Lorenti, G. Arena, and S. Coffa, Hydrogen Etching Influence on 4H-SiC Homo-Epitaxial Layer for High Power Device, Mater. Sci. Forum. 897 (2016) 71-74.

[7] Kwansei Gakuin University, Toyota Tsusho Corporation. (March 1, 2021). Kwansei Gakuin University and Toyota Tsusho Develop Innovative Process that Achieves "Zero Defects" in 6-Inch SiC Substrates - Supply of Samples to Device Manufacturers to Begin to Facilitate Early Mass Production [Press release]. https://global.kwansei.ac.jp/cms/kwansei_en/researchspotlight/20211020_プレスリリース英文02.pdf

[8] A. Fiocchi, C. A. Fortulan, L. Eduardo and A. Sanchez, Ultra-precision face grinding with constant pressure, lapping kinematics, and SiC grinding wheels dressed with overlap factor, Int J Adv Manuf Technol. 79 (2015) 1531-1543.

[9] K. Moeggenborg, M. Ju, Polish Scratch Simulation vs. Polish Tool Type, Mater. Sci. Forum. 1062 (2022) 175-179.

[10] X. Y. Wang, Y Li, S. J. Li, Study on the Impact of the Cutting Process of Wire Saw on SiC Wafers, Appl. Mech. Mater. 120 (2012) 593-597.